Chinese Journal of Aeronautics, (2014),27(6): 1544–1553

Chinese Society of Aeronautics and Astronautics
& Beihang University

Chinese Journal of Aeronautics

cja@buaa.edu.cn
www.sciencedirect.com

Real-time total system error estimation: Modeling and application in required navigation performance

Fu Li, Zhang Jun *, Li Rui

National Key Laboratory of CNS/ATM, School of Electronic and Information Engineering, Beihang University, Beijing 100191, China

Received 4 December 2013; revised 12 February 2014; accepted 25 April 2014
Available online 19 October 2014

KEYWORDS

Aviation;
Estimation;
Navigation;
Required navigation performance;
Total system error

Abstract In required navigation performance (RNP), total system error (TSE) is estimated to provide a timely warning in the presence of an excessive error. In this paper, by analyzing the underlying formation mechanism, the TSE estimation is modeled as the estimation fusion of a fixed bias and a Gaussian random variable. To address the challenge of high computational load induced by the accurate numerical method, two efficient methods are proposed for real-time application, which are called the circle tangent ellipse method (CTEM) and the line tangent ellipse method (LTEM), respectively. Compared with the accurate numerical method and the traditional scalar quantity summation method (SQSM), the computational load and accuracy of these four methods are extensively analyzed. The theoretical and experimental results both show that the computing time of the LTEM is approximately equal to that of the SQSM, while it is only about 1/30 and 1/6 of that of the numerical method and the CTEM. Moreover, the estimation result of the LTEM is parallel with that of the numerical method, but is more accurate than those of the SQSM and the CTEM. It is illustrated that the LTEM is quite appropriate for real-time TSE estimation in RNP application.

1. Introduction

With the development of the next generation air transportation system (NextGen), performance based navigation (PBN) is required to implement in the next few years by the International Civil Aviation Organization (ICAO).[1] Required navigation performance (RNP) is a core component of PBN, which plays an important role in guaranteeing flight efficiency and safety.[2]

RNP defines a total of four performance parameters: accuracy, integrity, continuity and availability. Integrity is especially important for aviation safety, which indicates the ability of a timely alert to a user in the presence of a system failure or an excessive error.[3–6] For RNP operation, total system error (TSE) is estimated to compare with the navigation specification to judge whether an aircraft satisfies the RNP requirement or not. Since the true position is unknown, TSE obeys a certain probability distribution during a flight. Consequently, real-time TSE should be estimated to compare with the threshold to provide a timely warning when TSE exceeds

* Corresponding author. Tel.: +86 10 82338282.
E-mail address: buaazhangjun@vip.sina.com (J. Zhang).

Peer review under responsibility of Editorial Committee of CJA.

ELSEVIER Production and hosting by Elsevier

http://dx.doi.org/10.1016/j.cja.2014.10.021

the bounds. It may cause false alarms if the estimation is conservative. Otherwise, it may cause missed warnings, which is hazardous to flight safety. Moreover, TSE estimation methods should be efficient to meet the real-time requirement.

Currently, the existing TSE estimation methods include the root sum square method (RSSM) and the scalar quantity summation method (SQSM). The RSSM obtains the distribution of TSE as a Gaussian with a standard deviation equal to the root sum square of the standard deviations of flight technical error (FTE) and navigation system error (NSE).[7,8] As the distributional property of TSE cannot accurately reflect the true TSE of a current moment, it may be unsuitable for real-time application. The SQSM regards FTE and NSE as scalar quantities and sums them to estimate TSE.[9] Nevertheless, the method does not distinguish the lateral and longitudinal components of TSE, which may lead to conservative results when the true FTE and NSE are in different directions.

In the works above, TSE is estimated as a simple sum of FTE and NSE, while the formation mechanism of TSE is rarely discussed. The goal of TSE estimation is to compute a statistical bound of TSE so as to guarantee that the probability of the true TSE exceeding the said number is smaller than the performance requirement. A similar concept is the protection level (PL), which has been widely used in NSE to describe a bound of the horizon/vertical positioning error linked to the integrity risk. In this paper, research on an accurate and real-time TSE estimation method for RNP application is presented.

2. TSE estimation model

In this section, the properties of FTE and NSE are analyzed to obtain the formation mechanism of TSE. Then, the TSE estimation is modeled as the estimation fusion of a fixed bias and a Gaussian random variable.

TSE is defined as the deviation of a flight true position away from the desired path, which mainly consists of path definition error (PDE), FTE and NSE, as shown in Fig. 1. On the assumption that PDE is negligible, TSE is the integration of FTE and NSE.[10]

To estimate TSE accurately, it is essential to know the properties of the two main components, i.e., FTE and NSE. Recently, FTE has been investigated,[11] and can be obtained from a flight management system (FMS) timely and accurately.[12,13] NSE varies with navigation modes. With the development of global navigation satellite system (GNSS), the GNSS-based navigation mode is becoming an inevitable trend in the future. Consequently, the GNSS-based real-time TSE estimation is researched in this section, which can be easily extended to other navigation modes. The NSE of the GNSS mode obeys a Gaussian distribution, whose covariance matrix is decided by the geometrical configuration and the pseudorange errors.[14]

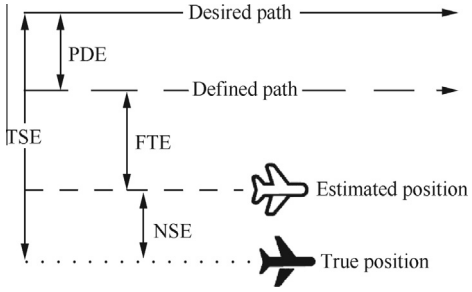

Fig. 1 Composition of TSE.

In this paper, real data of RNP during an approach phase are utilized to valid the properties of FTE and NSE. As shown in Fig. 2(a), the figure shows that the difference between FTE and FMS observations is less than 0.05 m. With FMS observations, FTE can be obtained as a bias error at each sample time. The Gaussian assumption is simple and convenient for calculation, which has been widely used to describe the GNSS navigation error. As shown in Fig. 2(b), the normal quantile–quantile (Q–Q) plot of NSE indicates that NSE is close to a Gaussian distribution, although it does not strictly obey the distribution as imperfect data. Consequently, the problem of real-time TSE estimation can be transformed into the estimation fusing of a bias error and a Gaussian random variable.

The NSE of GNSS positioning obeys Gaussian distribution $N(\mathbf{0}, \boldsymbol{\Sigma})$, where $\boldsymbol{\Sigma}$ is the covariance matrix of the distribution. $\boldsymbol{\Sigma}$ with N_s visual satellites can be obtained as: $\boldsymbol{\Sigma} = \sigma_p^2(\boldsymbol{H}^T\ \boldsymbol{H})^{-1}$, where σ_p is the standard deviation of pseudorange errors and $\boldsymbol{H} \in \mathbf{R}^{Ns\times 4}$ is the observation matrix. As matrix $\boldsymbol{H}$ is calculated by the N_s directions from the receiver to the visual satellites, it is usually called the geometrical configuration matrix. To obtain the parameters of the Gaussian distribution of NSE, the geometrical configuration and the pseudorange errors should be applied.

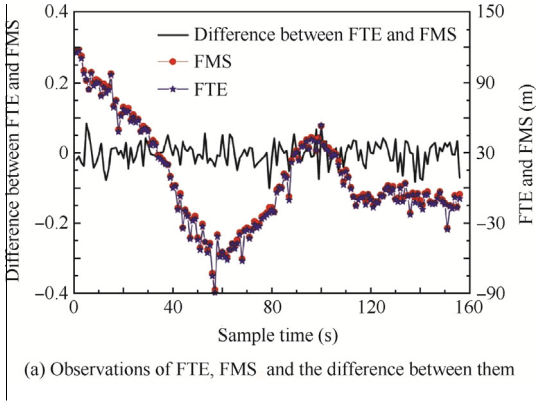

(a) Observations of FTE, FMS and the difference between them

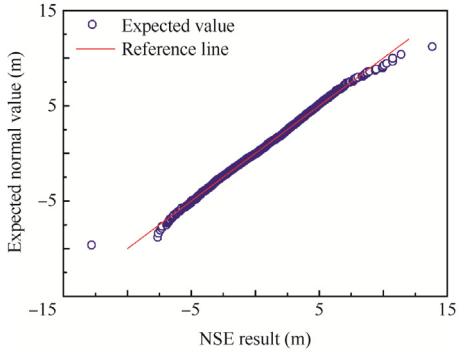

(b) Normal Q-Q plot of GNSS-based NSE result

Fig. 2 Properties of FTE and NSE with real data of one approach phase.

The 2-by-2 covariance matrix of the East–North coordinates of the GNSS-based NSE can be obtained as $\boldsymbol{\Sigma}_{\mathrm{EN}} \in \mathbf{R}^{2\times2}$.[15] In RNP, TSE of an aircraft is required to be less than the threshold $T_{\mathrm{h}} \in \mathbf{R}^{+}$ with the probability $P_{\mathrm{RNP}} \in (0,1)$. To achieve this, in this paper, the equal probability ellipse of NSE is applied as[16,17]

$$(\boldsymbol{x}_{\mathrm{EN}} - \boldsymbol{\mu}_{\mathrm{EN}})^{\mathrm{T}} \boldsymbol{\Sigma}_{\mathrm{EN}}^{-1} (\boldsymbol{x}_{\mathrm{EN}} - \boldsymbol{\mu}_{\mathrm{EN}}) = K^2 \tag{1}$$

where $\boldsymbol{x}_{\mathrm{EN}} \in \mathbf{R}^2$ and $\boldsymbol{\mu}_{\mathrm{EN}} \in \mathbf{R}^2$ are the true position of the aircraft and the positioning result of GNSS in the East–North coordinates, respectively; $K \in \mathbf{R}^{+}$ is the constant to be determined by the probability P_{RNP}.

As shown in Table 1,[2] for a given flight phase, the RNP navigation specification is designated as RNP-x_{RNP}, where x_{RNP} is a metric in nautical mile, e.g., RNP-1.

In RNP, there are two navigation requirements associated with TSE, namely:

(1) *Accuracy:* the true TSE remains equal to or less than x_{RNP} for 95% of the flight time.
(2) *Integrity:* the probability that the true TSE of the aircraft exceeds $2x_{\mathrm{RNP}}$ without annunciation is less than 10^{-5}.

According to the confidence probability of a Gaussian distribution, in accuracy of RNP-x_{RNP}, $T_{\mathrm{h}} = x_{\mathrm{RNP}}$, $P_{\mathrm{RNP}} = 95\%$ and $K = 1.96$, while in integrity of RNP-x_{RNP}, $T_{\mathrm{h}} = 2x_{\mathrm{RNP}}$, $P_{\mathrm{RNP}} = 99.999\%$ and $K = 4.41$. The navigation performance of RNP within a defined airspace is required to support the navigation specification.

Then, the equal probability ellipse is obtained according to Eq. (1). Given an estimated position o, the aircraft's true position $\boldsymbol{x}_{\mathrm{EN}}$ has a probability of P_{RNP} located in the equal possibility ellipse, whose center, semi-major axis, and semi-minor axis are o, $a \in \mathbf{R}^{+}$ and $b \in \mathbf{R}^{+}$, respectively, as shown in Fig. 3(a).

The aim of TSE estimation is to calculate the length between the true position of the aircraft and the desired path accurately. As discussed above, TSE estimation is equal to the estimation fusion of a fixed bias and a Gaussian random variable. To make it convenient to utilize the Gaussian random variable, the coordinate system must first be rotated to remove the off-diagonal correlation of the ellipse.[18] The covariance matrix $\boldsymbol{\Sigma}_{\mathrm{EN}}$ can be diagonalized as

$$\boldsymbol{\Sigma}_{\mathrm{EN}} = \boldsymbol{V}\boldsymbol{\Lambda}\boldsymbol{V}^{\mathrm{T}} \tag{2}$$

where $\boldsymbol{\Lambda} = \mathrm{diag}(\lambda_a, \lambda_b)$ is diagonal matrix, in which λ_a and λ_b are the eigenvalues of $\boldsymbol{\Sigma}_{\mathrm{EN}}$; $\boldsymbol{V}$ is orthonormal matrix, which can be denoted as $\begin{bmatrix} \cos\phi & -\sin\phi \\ \sin\phi & \cos\phi \end{bmatrix}$, where $\phi \in (0,2\pi)$ is the corresponding rotation angle from the rotated coordinate to the East–North coordinates. As shown in Fig. 3(b), in the rotated coordinate system, the desired path is transformed into line $y = kx$ (where $k = \cot\phi$ is the slope of the line) from the y axis. Without loss of generality, it is assumed that $k \in \mathbf{R}^{+}$. The center of the ellipse is transferred by $\boldsymbol{\mu}'_{\mathrm{EN}} = [x_0, \quad y_0]^{\mathrm{T}}$ after the rotation, and the semi-major and semi-minor axes are $a = K\sqrt{\lambda_a}$ and $b = K\sqrt{\lambda_b}$, respectively. Then, the ellipse in the rotated coordinate system can be obtained as

$$\frac{(x-x_0)^2}{a^2} + \frac{(y-y_0)^2}{b^2} = 1 \tag{3}$$

As shown in Fig. 3(b), the true position of the aircraft should be located between the envelope lines l_1: $y = kx + d$ and l_2: $y = kx - d$ (where $d \in \mathbf{R}^{+}$ is the intercept of the line) with a probability of P_{RNP} to guarantee that the aircraft is inside the RNP bounds. The value of $1 - P_{\mathrm{RNP}}$ is defined as TSE that is outside the envelope lines instead of the bounds. To achieve this, the probability in the purple zone is applied to compensate for the probability in the yellow zone of the ellipse, i.e., $P_{\mathrm{purple}} = P_{\mathrm{yellow}}$. According to the property of the ellipse $P_{\mathrm{yellow}} + P_{\mathrm{blue}} = P_{\mathrm{RNP}}$, we can obtain

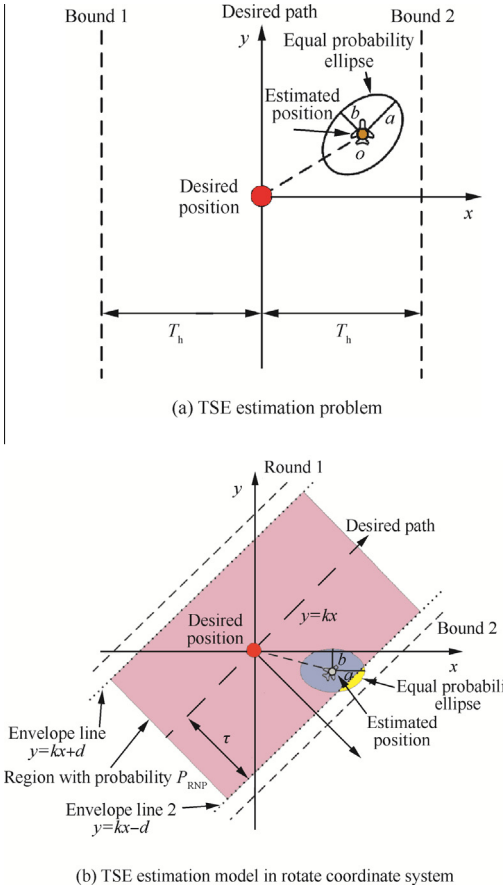

Fig. 3 TSE estimation model.

Table 1 Navigation specification in different flight phases.

Navigation specification	En route oceanic/remote	Arrive	Initial	Interm	Final	Missed	Depart
RNP-4	4						
RNP-1		1	1	1		1	1
RNP approach			1	1	0.3	1	
RNP authorization required approach			0.1–1	0.1–1	0.1–0.3	0.1–1	

$$P_{\text{purple}} + P_{\text{blue}} = P_{\text{RNP}} \tag{4}$$

where P_{blue} is the probability in the blue zone of the ellipse. Considering the property of NSE, its Gaussian distribution in the rotated coordinate system can be denoted as

$$p(x,y) = \frac{1}{2\pi\sigma_a\sigma_b} \times \exp\left[-\frac{(x-x_0)^2}{2\sigma_a^2} - \frac{(y-y_0)^2}{2\sigma_b^2}\right] \tag{5}$$

where $\sigma_a = \sqrt{\lambda_a}$, and $\sigma_b = \sqrt{\lambda_b}$ are the standard deviations in the two axes, respectively.

The region between l_1 and l_2 is given by:

$$\boldsymbol{D} = \{(x,y)|(y - kx - d) \in \mathbf{R}^-,\ (y - kx + d) \in \mathbf{R}^+\}. \tag{6}$$

As the slope k can be obtained in the rotation, the probability that the aircraft locates in the region $\boldsymbol{D}$ is a function of d:

$$P_{\boldsymbol{D}}(d) = \iint_{\boldsymbol{D}} p(x,y)\mathrm{d}x\mathrm{d}y \tag{7}$$

The distance between the envelope line l_1 or l_2 to the desired path is obtained as

$$\boldsymbol{L} = \frac{d}{\sqrt{1+k^2}} \tag{8}$$

If $\boldsymbol{L}$ is larger than the threshold T_{h}, it means that the two envelope lines l_1 and l_2 in Fig. 3(b) are outside bound 1 and bound 2. In this case, we should give a TSE warning to the user. We can obtain:

$$d = \boldsymbol{L}\sqrt{1+k^2} \tag{9}$$

Substitute Eq. (9) into Eq. (7), and a function $f(\xi)$ is defined as

$$f(\xi) = P_{\boldsymbol{D}}\left(\xi\sqrt{1+k^2}\right) - P_{\text{RNP}} \tag{10}$$

where ξ is the variable of the function.

The evaluated TSE is the solution of $f(\xi) = 0$. If the solved TSE is less than the threshold T_{h} in RNP-x_{RNP}, it is normal flight at the moment. Otherwise, the envelope would exceed the bounds of RNP, and a warning should be provided by the system.

3. Approaches and comparisons

In this section, the numerical method is firstly proposed to solve the TSE model. However, it is complex and time-consuming, which may not meet the real-time requirement. Then, the traditional SQSM based on the model is also presented, while it is conservative. Based on the model, two efficient TSE estimation methods, i.e., the circle tangent ellipse method (CTEM) and the line tangent ellipse method (LTEM), are proposed for real-time application. Finally, these four methods are compared in terms of accuracy and computational load.

3.1. Numerical method for solving the model

To solve the model, it is necessary to get the probability function $P_{\boldsymbol{D}}(d)$. Substituting Eqs. (5) and (6) into Eq. (7) yields:

$$P_{\boldsymbol{D}}(d) = \int_{-\infty}^{+\infty} \frac{1}{\sqrt{2\pi}\sigma_a} \exp\left[-\frac{(x-x_0)^2}{2\sigma_a^2}\right]\mathrm{d}x \cdot \int_{kx-d}^{kx+d} \frac{1}{\sqrt{2\pi}\sigma_b} \exp\left[-\frac{(y-y_0)^2}{2\sigma_b^2}\right]\mathrm{d}y \tag{11}$$

Denote the cumulative distribution function of a normal distribution as $\Phi(\mu) = \frac{1}{\sqrt{2\pi}}\int_{-\infty}^{\mu} \exp\left(-\frac{\rho^2}{2}\right)\mathrm{d}\rho$, so Eq. (11) can be written as

$$P_{\boldsymbol{D}}(d) = \int_{-\infty}^{+\infty} \frac{1}{\sqrt{2\pi}\sigma_a} \exp\left[-\frac{(x-x_0)^2}{2\sigma_a^2}\right]\Phi\left(\frac{kx+d-y_0}{\sigma_b}\right)\mathrm{d}x - \int_{-\infty}^{+\infty} \frac{1}{\sqrt{2\pi}\sigma_a} \exp\left[-\frac{(x-x_0)^2}{2\sigma_a^2}\right]\Phi\left(\frac{kx-d-y_0}{\sigma_b}\right)\mathrm{d}x \tag{12}$$

It is noted that $v = (x - x_0)/\sigma_a$. By applying the stepwise integration, we can obtain:

$$P_{\boldsymbol{D}}(d) = \underbrace{\Phi(v)\left[\Phi\left(\frac{kx_0 + k\sigma_a v + d - y_0}{\sigma_b}\right) - \Phi\left(\frac{kx_0 + k\sigma_a v - d - y_0}{\sigma_b}\right)\right]\Big|_{v=-\infty}^{v=\infty}}_{P_1(d)} \underbrace{- \int_{-\infty}^{+\infty} \frac{k\sigma_a}{\sqrt{2\pi}\sigma_b}\Phi(v)\left(\mathrm{e}^{-\frac{1}{2}\left(\frac{kx_0+k\sigma_a v+d-y_0}{\sigma_b}\right)^2} - \mathrm{e}^{-\frac{1}{2}\left(\frac{kx_0+k\sigma_a v-d-y_0}{\sigma_b}\right)^2}\right)\mathrm{d}v}_{P_2(d)} \tag{13}$$

As shown in Eq. (13), the probability function $P_{\mathscr{D}}(d)$ is composed of $P_1(d)$ and $P_2(d)$.

(1) If $k = 0$, then $P_2(d) = 0$, and thus:

$$P_{\boldsymbol{D}}(d) = P_1(d) = \Phi\left(\frac{d-y_0}{\sigma_b}\right) - \Phi\left(\frac{-d-y_0}{\sigma_b}\right) \tag{14}$$

(2) If $k \neq 0$, then $P_1(d) = 0$, and thus:

$$P_{\boldsymbol{D}}(d) = P_2(d) = -\int_{-\infty}^{+\infty} \frac{k\sigma_a}{\sqrt{2\pi}\sigma_b}\Phi(v)\exp\left(-\frac{1}{2}\left(\frac{kx_0+k\sigma_a v+d-y_0}{\sigma_b}\right)^2\right)\mathrm{d}v + \int_{-\infty}^{+\infty} \frac{k\sigma_a}{\sqrt{2\pi}\sigma_b}\Phi(v)\exp\left(-\frac{1}{2}\left(\frac{kx_0+k\sigma_a v-d-y_0}{\sigma_b}\right)^2\right)\mathrm{d}v \tag{15}$$

Define

$$R(d)=\begin{cases}\Phi\left(\frac{d-y_0}{\sigma_b}\right) & k=0\\ -\int_{-\infty}^{+\infty}\frac{k\sigma_a}{\sqrt{2\pi}\sigma_b}\Phi(v)\exp\left(-\frac{1}{2}\left(\frac{kx_0+k\sigma_a v+d-y_0}{\sigma_b}\right)^2\right)\mathrm{d}v & k\neq 0\end{cases} \tag{16}$$

Then, we can obtain:

$$P_{\boldsymbol{D}}(d)=R(d)-R(-d) \tag{17}$$

Substituting Eq. (17) into Eq. (10) yields:

$$f(\xi)=R\left(\xi\sqrt{1+k^2}\right)-R\left(-\xi\sqrt{1+k^2}\right)-P_{\mathrm{RNP}} \tag{18}$$

To solve $f(\xi)=0$ in Eq. (18), the numerical method is required.[19] The solution is denoted as τ_{NM}. The result of the model is obviously an exact solution, as it exceeds the true TSE with a probability of P_{RNP} strictly. However, the solving process is complex and time-consuming, which may not meet the real-time requirement. Consequently, it is necessary to investigate more efficient approaches for RNP application.

3.2. Efficient approaches for RNP application

3.2.1. SQSM

The conventional SQSM regards FTE and NSE as scalar quantities and sums them to estimate TSE,[10] as shown in Fig. 4(a). The calculation time is negligible and the TSE estimation result is obtained as

$$\tau_{\mathrm{SQSM}}=\eta+\max\{a,b\}. \tag{19}$$

where η is the value of FTE, which can be obtained by calculating the distance between the center of the ellipse center (x_0, y_0) and the desired path $y=kx$, i.e., $\eta=|y_0-kx_0|/\sqrt{1+k^2}$. Then, TSE estimation of the SQSM is obtained as

$$\tau_{\mathrm{SQSM}}=\frac{|y_0-kx_0|}{\sqrt{1+k^2}}+\max\{a,b\} \tag{20}$$

TSE is inherently the combination of the FTE vector and the NSE vector, which will be less than the sum of the corresponding scalar quantities if FTE and NSE are in different directions. Thus, the result of the SQSM is conservative, and may cause false alarms.

3.2.2. CTEM

In this section, the CTEM is proposed to obtain real-time TSE estimation. Inspired by the model, a circle $O(r)$ with the expected point as the center which is tangent to the ellipse is applied to obtain the envelope of TSE with a probability of P_{RNP}, as shown in Fig. 4(b). The farthest point on the ellipse from the expected point should be tangent on the circle, and thus we consider the following problem:

$$\begin{aligned}&\max_{(x_{\mathrm{f}},y_{\mathrm{f}})} r^2=x_{\mathrm{f}}^2+y_{\mathrm{f}}^2\\ &\text{s.t. }\frac{(x_{\mathrm{f}}-x_0)^2}{a^2}+\frac{(y_{\mathrm{f}}-y_0)^2}{b^2}=1\end{aligned} \tag{21}$$

where $r\in\mathbf{R}^+$ is the radius of the circle $O(r)$. Denote $x_{\mathrm{f}}=-x_0+a\cos\theta$, $y_{\mathrm{f}}=y_0+b\sin\theta$, and $\theta\in(0,2\pi)$. Substituting them into Eq. (21) yields:

$$\max_{\theta} r^2(\theta)=(x_0+a\cos\theta)^2+(y_0+b\sin\theta)^2 \tag{22}$$

The farthest point is required to satisfy $\partial r(\theta)/\partial\theta=0$, so that

$$\frac{\partial r(\theta)}{\partial\theta}=(b^2-a^2)\cos\theta\sin\theta-ax_0\sin\theta+by_0\cos\theta=0 \tag{23}$$

(1) If $a=b$, the ellipse degenerates into a circle, and Eq. (23) can be written as

$$-x_0\sin\theta+y_0\cos\theta=0 \tag{24}$$

then $\sin\theta=y_0/\sqrt{x_0^2+y_0^2}$ and $\cos\theta=x_0/\sqrt{x_0^2+y_0^2}$.

Substituting Eq. (24) into Eq. (22) yields:

$$r(\theta)=\sqrt{x_0^2+y_0^2+2a(x_0\cos\theta+y_0\sin\theta)+a^2}=\sqrt{x_0^2+y_0^2}+a \tag{25}$$

(2) If $a\neq b$, denote $t=\tan(\theta/2)$, and then $\sin\theta=2t/(1+t^2)$ and $\cos\theta=(1-t^2)/(1+t^2)$. We have:

$$\frac{\partial r(\theta)}{\partial\theta}=(b^2-a^2)\frac{2t(1-t^2)}{(1+t^2)^2}-ax_0\frac{2t}{1+t^2}+by_0\frac{1-t^2}{1+t^2}=0 \tag{26}$$

Eq. (26) can be transformed into a 4-order equation:

$$by_0t^4+2(ax_0-a^2+b^2)t^3+2(ax_0+a^2-b^2)t-by_0=0 \tag{27}$$

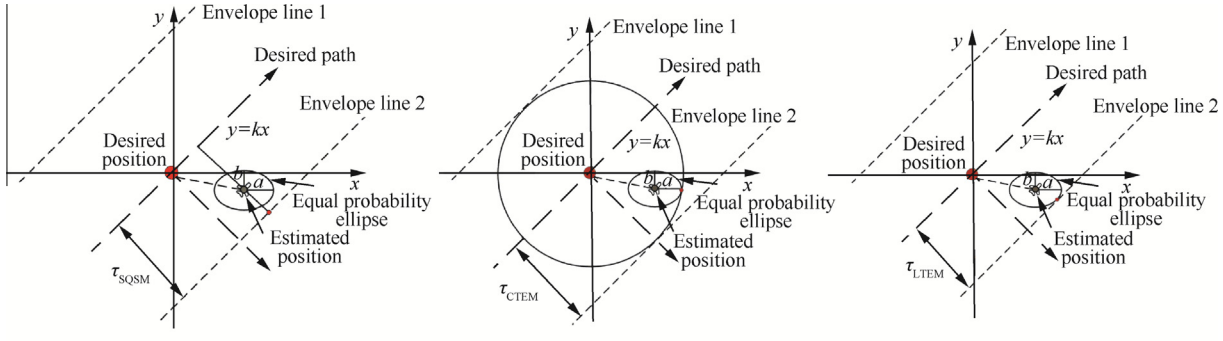

(a) SQSM (b) CTEM (c) LTEM

Fig. 4 Three kinds of efficient TSE estimation approaches.

a. If $y_0 = 0$, Eq. (27) is degenerated into a 3-order equation:

$$(ax_0 - a^2 + b^2)t^3 + (ax_0 + a^2 - b^2)t = 0 \tag{28}$$

whose three solutions are $t_1 = 0$ and $t_{2,3} = \pm\sqrt{(-ax_0 - a^2 + b^2)/(ax_0 - a^2 + b^2)}$.

b. If $y_0 \neq 0$, transform the first coefficient of Eq. (27) into 1 to obtain:

$$t^4 + \frac{2(ax_0 - a^2 + b^2)}{by_0}t^3 + \frac{2(ax_0 + a^2 - b^2)}{by_0}t - 1 = 0 \tag{29}$$

The solutions of Eq. (29) are also the eigenvalues of the matrix as follows:

$$\boldsymbol{A} = \begin{bmatrix} -\frac{2(ax_0 - a^2 + b^2)}{by_0} & 0 & -\frac{2(ax_0 + a^2 - b^2)}{by_0} & -1 \\ 1 & 0 & 0 & 0 \\ 0 & 1 & 0 & 0 \\ 0 & 0 & 1 & 0 \end{bmatrix} \tag{30}$$

Considering that there are two extreme points on the ellipse, i.e., the maximum and the minimum, the matrix $\boldsymbol{A}$ has and only has two real eigenvalues $t_1 = \lambda_1$ and $t_2 = \lambda_2$.

Thus, the solution of the Eq. (23) can be obtained as

$$\theta_i = 2\arctan t_i \ (i = 1, 2, \ldots, N_s) \tag{31}$$

where N_s is the total number of real solutions of Eq. (23). Then, the parameters θ_i are substituted into Eq. (21) to obtain the maximum solution:

$$\tau_{CTEM} = \max_i r(\theta_i) \tag{32}$$

As discussed above, it is illustrated that TSE estimation of the CTEM is simpler than that of the numerical method. According to the definition of TSE, the points on the same line parallel with the desired path have the same TSE. However, when (x', y') and (x_0, y_0) $((x', y') \neq (x_0, y_0))$, which are the points on line l_3: $y = kx + y_0 - kx_0$, are substituted into Eq. (30), respectively, the solutions of the CTEM are obviously different. Thus, the TSE estimation result of the CTEM is negatively impacted by the positioning result.

3.2.3. LTEM

To obtain TSE accurately and avoid the impact of the positioning result, the LTEM is proposed in this paper. As shown in Fig. 4(c), based on the TSE model, the distance between the envelope lines is properly enlarged to make one of the lines tangent to the circle. The distance between the new parallel lines is calculated to meet the real-time requirement. As the lines are parallel to the desired path, TSE is not impacted by the positioning result.

The tangent point (x_t, y_t) is on the ellipse and should satisfy:

$$\frac{(x_t - x_0)^2}{a^2} + \frac{(y_t - y_0)^2}{b^2} = 1 \tag{33}$$

The differential of Eq. (33) is given by:

$$\frac{x_t - x_0}{a^2}\mathrm{d}x_t + \frac{y_t - y_0}{b^2}\mathrm{d}y_t = 0 \tag{34}$$

As the tangent line is parallel to the desired path, the slope is obtained as

$$\frac{\mathrm{d}y_t}{\mathrm{d}x_t} = k \tag{35}$$

(1) If $k = 0$ or $k = \infty$, i.e., the axis of the ellipse is parallel or perpendicularity to the desired line, TSE can be obtained as

$$\tau_{LTEM} = b + y_0, \quad \text{or } \tau_{LTEM} = a + x_0 \tag{36}$$

which is the same as the result of the SQSM.

(2) If $k \neq 0$ and $k \neq \infty$, the farther solutions are obtained by solving the combination of Eq. (33)–(35):

$$\begin{cases} y_t = y_0 \pm \frac{b^2}{\sqrt{k^2a^2 + b^2}} \\ x_t = x_0 \mp \frac{ka^2}{\sqrt{k^2a^2 + b^2}} \end{cases} \tag{37}$$

TSE can be obtained by calculating the distance from the tangent point to the desired path:

$$\tau_{LTEM} = \frac{|y_0 - kx_0 \pm \sqrt{k^2a^2 + b^2}|}{\sqrt{1 + k^2}} \tag{38}$$

To obtain the envelope, the larger solution of the LTEM is selected as the final TSE estimation result. As shown in Fig. 4(c), we have $y_0 - kx_0 \leqslant 0$, and thus TSE estimation can be obtained as

$$\tau_{LTEM} = \frac{kx_0 - y_0 + \sqrt{k^2a^2 + b^2}}{\sqrt{1 + k^2}} \tag{39}$$

Since the difference between the LTEM and the numerical method is just a fraction of the ellipse, the LTEM result is very close to the numerical method result. The advantage of the LTEM is that it can obtain TSE with much less computing.

3.3. Approaches comparison

In this section, the accuracies and computational loads of the numerical method, the SQSM, the CTEM, and the LTEM are deducted and compared to assess which method is most appropriate for RNP application.

3.3.1. Accuracy

(1) $\tau_{NM} < \tau_{LTEM}$

As shown in Fig. 3(c), during the process of the numerical method, the probability in the purple region is applied to compensate the probability in the yellow region of the ellipse. Thus, τ_{NM} should be the distance between a secant of the ellipse and the desired path. The result of the LTEM is the farther tangent of the ellipse. Thus, the conclusion can be obtained easily as

$$\tau_{NM} < \tau_{LTEM} \tag{40}$$

(2) $\tau_{SQSM} \geqslant \tau_{LTEM}$

When compared with Eq. (20) and Eq. (39),

$$\tau_{SQSM} - \tau_{LTEM} = \frac{kx_0 - y_0}{\sqrt{1+k^2}} + \max\{a,b\} - \frac{kx_0 - y_0 + \sqrt{k^2a^2+b^2}}{\sqrt{1+k^2}} \quad (41)$$

Then, we can obtain:

$$\tau_{SQSM} - \tau_{LTEM} = \max\{a,b\} - \frac{\sqrt{k^2a^2+b^2}}{\sqrt{1+k^2}} \geq 0 \quad (42)$$

If and only if $a = b$ or $k = \infty$, $a > b$ or $k = 0$, $a < b$, the equality holds.

(3) $\tau_{CTEM} \geqslant \tau_{LTEM}$

According to the property of the CTEM, we can obtain $\tau_{CTEM} \geq \sqrt{x_t^2 + y_t^2}$, and when combining it with Eq. (38) and the Cauchy inequality, we can obtain:

$$\tau_{LTEM} = \frac{|y_t - kx_t|}{\sqrt{1+k^2}} \leq \sqrt{x_t^2 + y_t^2} \leq \tau_{CTEM} \quad (43)$$

If and only if $y_t/x_t = -1/k$ and the tangent point $(x_t, y_t) = (x_f, y_f)$, the equality holds.

It can be obtained from Eq. (37) that $y_t/x_t = -1/k$ is equivalent to the center of the ellipse (x_0, y_0) which satisfies:

$$x_0 + ky_0 = \frac{k(b^2 - a^2)}{\sqrt{k^2a^2+b^2}} \quad (44)$$

Combined with Eq. (22), $(x_t, y_t) = (x_f, y_f)$ is equivalent to

$$(b^2 - a^2)k + \sqrt{k^2a^2+b^2}(x_0 + ky_0) = 0 \quad (45)$$

Substituting Eq. (44) into Eq. (45) yields:

$$2(b^2 - a^2)k = 0 \quad (46)$$

Thus, the solution of Eq. (45) is $k = 0$ or $a = b$. Substituting them into Eq. (44) yields:

$$x_0 + ky_0 = 0 \quad (47)$$

If $k = 0$, we can obtain $x_0 = 0$, and if $a = b$, then $x_0 + ky_0 = 0$. Thus, if and only if $k = 0$, $x_0 = 0$ or $a = b$, $x_0 + ky_0 = 0$, the equality in $\tau_{CTEM} \geqslant \tau_{LTEM}$ holds.

(4) τ_{SQSM} and τ_{CTEM}

From Eqs. (20)–(22), $\tau_{SQSM} = \tau_{CTEM}$ if and only if:

$$\begin{cases} \frac{|y_0 - kx_0|}{\sqrt{1+k^2}} + \max\{a,b\} = \sqrt{(x_0 + a\cos\theta)^2 + (y_0 + b\sin\theta)^2} \\ (b^2 - a^2)\cos\theta\sin\theta - ax_0\sin\theta + by_0\cos\theta = 0 \end{cases} \quad (48)$$

As the format of the parameter θ is very complex, it is difficult to know the relationship between τ_{SQSM} and τ_{CTEM}. Thus, a simple case is considered, i.e., $y_0 = 0$. Substituting $y_0 = 0$ into Eq. (20) and Eq. (32) yields:

$$\tau_{SQSM} = \frac{kx_0}{\sqrt{1+k^2}} + \max\{a,b\} \quad (49)$$

$$\tau_{CTEM} = x_0 + a \quad (50)$$

Table 2 Comparison between the four TSE estimation methods.

Method	TSE estimation	Accuracy	Computing load
Numerical method	Eq. (18)	Very accurate	Large
SQSM	Eq. (20)	Conservative	Small
CTEM	Eq. (32)	Conservative	Medial
LTEM	Eq. (39)	Accuracy	Small

If $b > a + x_0(\sqrt{1+k^2} - k)/\sqrt{1+k^2}$, $\tau_{SQSM} > \tau_{CTEM}$. Else, $\tau_{SQSM} \leqslant \tau_{CTEM}$. It is illustrated that the relation between τ_{SQSM} and τ_{CTEM} is uncertain which is affected by the parameters.

Conclusively, the relationship between the estimated TSEs of the four methods is:

$$\tau_{NM} < \tau_{LTEM} \leq \tau_{CTEM}, \tau_{SQSM} \quad (51)$$

As τ_{NM} is the solution of the TSE estimation model, it is the exact TSE estimation. Eq. (51) shows that τ_{LTEM} is much closer to τ_{NM} when compared with τ_{CTEM} and τ_{SQSM}. It is illustrated that τ_{CTEM} and τ_{SQSM} are more conservative than τ_{LTEM}.

3.3.2. Computational load

Considering the real-time requirement, the computational load is another indicator to evaluate the performances of these methods. The numerical method is complex and may not meet the real-time requirement. The CTEM may also suffer from complex calculation due to the matrix decomposing. Compared with these two methods, the conventional SQSM and the proposed LTEM are quite simpler and more efficient.

To generalize the discussion above, the comparison between these TSE estimation methods is shown in Table 2. The most accurate TSE estimation result can be obtained by the numerical method, while it is very time-consuming. Although the SQSM is fast, it is conservative, which may cause false alarms. The CTEM is medial when compared with the two methods above, while it is negatively affected by the positioning result. The LTEM is accurate and efficient, which is relatively suitable for real-time TSE estimation in RNP.

4. Experimental results and discussions

With simulated data and real data, three separate experiments are designed to evaluate the performances of these TSE estimation methods. The first experiment is to assess the computing time of these four methods by statistical analysis. The second experiment is to test the accuracy of these methods with simulated data. Finally, real data is applied to test the practical utility of these methods.

Our experiments are conducted using Matlab software in PC with a Core i7 CPU (2.93 GHz with 2 GB memory). The real data and simulated data are described as follows.

(1) Real data

The real test data were collected with a GNSS receiver (NovAtel DL-V3) during the approach phase of an aircraft at an airport in Chengdu, Sichuan Province in January 2013. The approach phase started from point (103.4352°, 30.38138°, 1100 m) in the longitude, latitude and height

(LLH) coordinate system and ended at point (103.46196°, 30.47895°, 547 m) in the LLH coordinate system. The total length of the flight phase was 11100 m.

The aircraft processed RNP-0.3 during the approach phase. For statistical evaluation, the dataset is utilized to test the accuracy performance of RNP (P_{RNP} = 95%), which has the length of 3063 s (composed by 19 sorties and about 160 s for each sortie). The real-time kinematic (RTK) technology is applied to provide positioning results up to centimeter-level accuracy,[20] which can be regarded as the true position of the aircraft.

(1) Simulated data

As it is difficult to obtain enough amount of real data to test the integrity performance of RNP (P_{RNP} = 99.999%), simulated data is set according to the process of the approach phase.

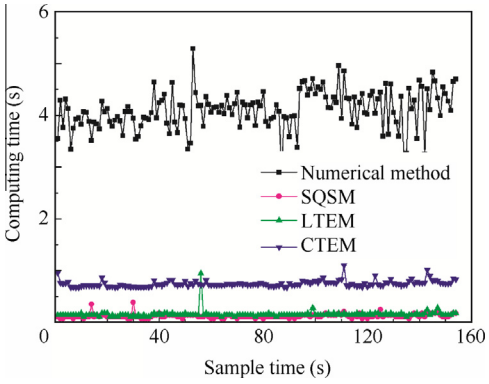

Fig. 5 Calculating times of four methods with real data during one approach phase.

Table 3 Performances of these four methods with simulated data.

Method	Exceed rate in RNP accuracy (%)	Exceed rate in RNP integrity (%)
Numerical method	95.03	99.99901
SQSM	97.75	99.99966
CTEM	97.16	99.99959
LTEM	95.32	99.99909

The simulated aircraft position is set to be the same as the real data. The GNSS data is simulated by using the broadcast ephemeris received by the GNSS monitor stations at the airport. The standard deviation of the pseudorange Gaussian noise is set as 12.5 m. To test the integrity performance of RNP, a total of 10^7 s of data is simulated.

4.1. Simulated data result

The calculating times of these four methods with the real data during one approach phase are shown in Fig. 5. It indicates that the mean calculating times of the LTEM and the SQSM are only 0.15 s, which is about 1/30 and 1/6 of those of the numerical method (4.6 s) and the CTEM (0.87 s), respectively. The LTEM and the SQSM are simple and their computing times can be neglected. The CTEM is slower due to the matrix decomposing. As the numerical method is complex, it is most time-consuming.

The accuracies of these four methods with the simulated data are shown in Table 3. The exceed rate is defined as the percentage of the estimated TSE that is larger than the real TSE. The result of the numerical method exceeds the real TSE with probabilities of 95.03% and 99.99901% in RNP accuracy and RNP integrity, respectively, which can be considered as the exact TSE estimation result. The reason is that the numerical method is the solution of the TSE estimation model. The result of the LTEM is approximately equal to that of the numerical method. However, as the exceed rates are much larger, the results of the SQSM and the CTEM are relatively conservative.

4.2. Real data results

The real data during the approach phase are applied to compare these four methods. With the amount limitation of the real data, P_{RNP} is only set to 95% to test these methods in RNP accuracy. As the curves of each sortie are almost the

Table 4 Performances of these four methods with real data.

Method	Computing time (s)	Exceed rate (%)
Numerical method	3.86	95.05
SQSM	0.13	97.25
CTEM	0.75	97.89
LTEM	0.16	95.06

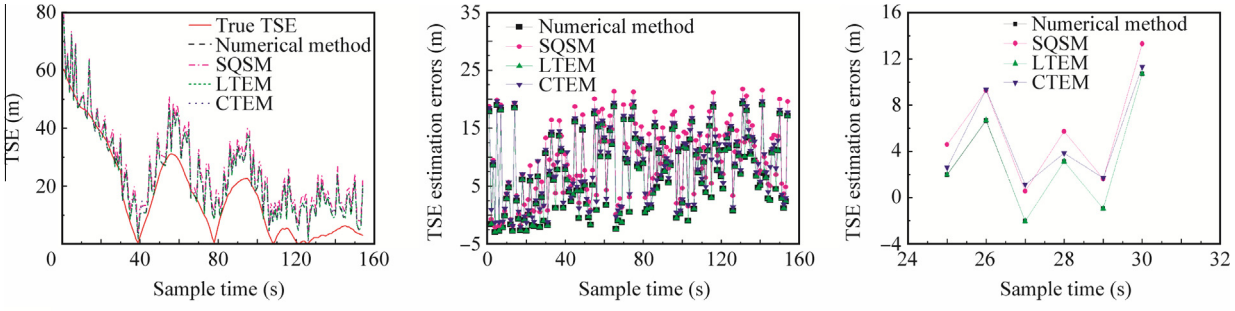

(a) True TSE and results of four TSE estimation methods

(b) TSE estimation errors of four methods in a sample time

(c) Partial enlarged view of Fig. 6(b)

Fig. 6 TSE estimation results in the approach phase.

same, we show only one of them for illustration. As shown in Fig. 6(a), the ascending order of the TSE estimation results of the four methods is the numerical method, the LTEM, the CTEM or the SQSM, which is consistent with the conclusion in Eq. (51). TSE estimation errors of these methods in the sample time are shown in Fig. 6(b), whose partial enlarged view is shown in Fig. 6(c). These results indicate that the error of the numerical method is the least, and the result of the LTEM is very approximate to that of the numerical method. However, the results of the SQSM and the CTEM are relatively more conservative.

The statistical results of the methods on the whole real data are shown in Table 4. The mean computing time of the LTEM is 0.16 s, almost the same as that of the SQSM (0.13 s), while it is about 1/30 and 1/6 of those of the numerical method (3.96 s) and the CTEM (0.75 s), respectively. The results of the numerical method and the LTEM are accurate and very close to each other, whose exceed rates are 95.05% and 95.06%, respectively. The results of the CTEM and the SQSM are relatively more conservative, whose exceed rates are 97.25% and 97.89%, respectively.

Conclusively, the LTEM is appropriate for real-time TSE estimation in RNP, since it is more accurate and efficient when compared with the other methods.

5. Conclusions

(1) By analyzing the formation mechanism of TSE, the real-time TSE estimation for RNP operation i modeled as the estimation fusion of fixed biases and Gaussian random variables.
(2) The CTEM and the LTEM are proposed for efficient TSE estimation to address the challenge of high computational load induced by the numerical method.
(3) Simulated data and real data during a RNP approach phase are utilized to evaluate the performances of these methods.
(4) The theoretical and experimental results show that the LTEM is more efficient and accurate when compared with the other methods, thereby is more appropriate for real-time TSE estimation in RNP application.

Acknowledgments

The presented research work was supported by the National Basic Research Program of China (No. 2010CB731805), the Foundation for Innovative Research Groups of the National Natural Science Foundation of China (No. 60921001), and the Special Fund for Basic Research on Scientific Instruments of China (No. 2011YQ04008301).

References

1. Zhao H, Xu X, Zhang J, Zhu Y, Yang C. Lateral flight technical error estimation model for performance based navigation. *Chin J Aeronaut* 2011;**24**(3):329–36.
2. International Civil Aviation Organization. *Performance-based navigation (PBN) manual*. 3rd ed. International Civil Aviation Organization; 2008.
3. Zhao X, Wang S, Zhang J, Fan Z, Min H. Real-time fault detection method based on belief rule base for aircraft navigation system. *Chin J Aeronaut* 2013;**26**(3):717–29.
4. Shao B, Liu J, Zhao R, Huang Z, Li R. A user differential range error calculating algorithm based on analytic method. *Chin J Aeronaut* 2011;**24**(6):762–7.
5. Schuster W, Bai J, Feng S, Ochieng W. Integrity monitoring algorithms for airport surface movement. *GPS Solutions* 2012;**16**(1):65–75.
6. Ochieng W, Sauer K, Walsh D, Brodin G, Griffin S, Denney M. GPS integrity and potential impact on aviation safety. *J Navig* 2003;**56**:51–65.
7. Guilloton A, Arethens J, Macabiau C, Escher A, Koenig D. A methodology to elaborate aircraft localization requirements for airport navigation. *Proceedings of the international technical meeting of the satellite division of the Institute of Navigation (ION GNSS)*. 2011 Sep 19–23; Portland, OR. Manassas, VA: The Institute of Navigation; 2011. p. 523–35.
8. Kim E. A coverage analysis methodology for APNT pseudolite ground network. *Proceedings of the international technical meeting of the satellite division of the Institute of Navigation (ION GNSS)*. 2011 Sep 19–23; Portland, OR. Manassas, VA: The Institute of Navigation; 2011. p. 495–507.
9. Stapleton D. A comparison of navigation by basic GPS lateral guidance to navigation by GPS/WAAS for various aircraft final approach categories. *Proceedings of the national technical meeting of the Institute of Navigation (ION NTM)*. 2005 May; San Diego, CA. Manassas, VA: The Institute of Navigation; 2005. p. 629–42.
10. Cassell R, Smith A. Development of required navigation performance (RNP) for airport surface movement guidance and control. *Proceedings of the 14th digital avionics systems conference*. 1995 Nov 5–9; Cambridge, MA. Piscataway, NJ: IEEE; 1995. p. 57–64.
11. Zhao H, Xu X, Zhang J, Zhu Y. Extended estimation method for lateral flight technical error of perturbed system in performance based navigation. *Aerosp Sci Technol* 2013;**30**(1):278–85.
12. Fujii N. A concept of CAT III GBAS requirement based on real-rime flight technical error estimation. *Proceedings of the international technical meeting of the satellite division of the Institute of Navigation (ION GNSS)*. 2007 Sep 25–28; Fort Worth, TX. Manassas, VA: The Institute of Navigation; 2007. p. 453–60.
13. Levy BS, Som P, Greenhaw R. Analysis of flight technical error on straight, final approach segments. *Proceedings of the 59th ION annual meeting*. 2003 Jun 23–25; Albuquerque, NM. Manassas, VA: The Institute of Navigation; 2003. p. 456–67.
14. Groves P. *Principles of GNSS, inertial, and multi-sensor integrated navigation systems*. 2nd ed. London/Boston: Artech House Publishers; 2013.
15. Grewal M, Weill L, Andrews A. *Global positioning system, inertial navigation, and integration*. 2nd ed. Hoboken, NJ: John Wiley & Sons Inc.; 2007.
16. Montillet J, Bonenberg L, Hancock C, Roberts G. On the improvements of the single point positioning accuracy with Locata technology. *GPS Solutions* 2014;**18**(2):273–82.
17. Forstner W, Moonen B. A metric for covariance matrices. In: Grafarend E, Krumm F, Schwarze V, editors. *Geodesy – the challenge of the 3rd millennium*. Berlin: Springer Berlin Heidelberg; 2003. p. 299–309.
18. Milner C, Ochieng W. A fast and efficient integrity computation for non-precision approach performance assessment. *GPS Solutions* 2010;**14**(2):193–205.
19. Gerald CF, Wheatley PO. *Applied numerical analysis*. MA: Addison-Wesley; 1989.
20. Mageed A, Mohamed K. Accuracy evaluation between GPS virtual reference station and GPS real time kinematic techniques. *World Appl Sci J* 2013;**24**(9):1154–62.

Fu Li is currently a Ph.D. student in the school of electronic and information engineering at Beihang University. His research interests include navigation sensor integration and integrity monitoring for aviation applications.

Zhang Jun is a professor in the school of electronic and information engineering at Beihang University. He was honored as an academician of the Chinese Academy of Engineering in 2013. His research interests include space communication and electronic system, modern air traffic management theory and application, traffic information engineering and control.

Li Rui received his Ph.D. degree in radio navigation from Beihang University. His work focuses on passive regional hybrid positioning system and augmented satellites navigation system. His main interests include TIS, INS, GNSS, and their integration applications.